Chemosphere 310 (2023) 136731

Contents lists available at ScienceDirect

Chemosphere

journal homepage: www.elsevier.com/locate/chemosphere

Microbial communities and metabolic pathways involved in reductive decolorization of an azo dye in a two-stage AD system

J.M.S. Oliveira [a,b], J.S. Poulsen [b], E. Foresti [a], J.L. Nielsen [b,*]

[a] Biological Processes Laboratory (LPB), São Carlos School of Engineering (EESC), University of São Paulo (USP), 1100 João Dagnone Avenue, 13563-120, São Carlos, SP, Brazil
[b] Center for Microbial Communities, Department of Chemistry and Bioscience, Aalborg University, Fredrik Bajers Vej 7H, DK-9220 Aalborg, Denmark

HIGHLIGHTS

- Color removal is negatively correlated with E_0 in the system.
- Azo dye decolorization was mainly associated with hydrogen producing pathways.
- Fermentative diversity improved decolorization efficiency in the 1st-stage.
- Acidogens in the 1st-stage were sensitive and shifted in the presence of the azo dye.
- Microbial communities in the 2nd-stage were more protected and remained similar.

GRAPHICAL ABSTRACT

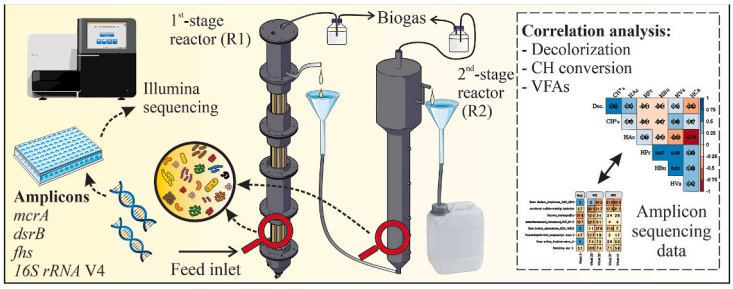

ARTICLE INFO

Handling Editor: Chang-Ping Yu

Keywords:
Biological wastewater treatment
Syntrophic acetate oxidation
Sulfate-reducing bacteria
Methanogens
Xenobiotics
Amplicon sequencing

ABSTRACT

Multiple stage anaerobic system was found to be an effective strategy for reductive decolorization of azo dyes in the presence of sulfate. Bulk color removal (56–90%) was achieved concomitant with acidogenic activity in the 1st-stage reactor (R1), while organic matter removal (≤100%) and sulfate reduction (≤100%) occurred predominantly in the 2nd-stage reactor (R2). However, azo dye reduction mechanism and metabolic routes involved remain unclear. The involved microbial communities and conditions affecting the azo dye removal in a two-stage anaerobic digestion (AD) system were elucidated using amplicon sequencing (*16S rRNA*, *fhs*, *dsrB* and *mcrA*) and correlation analysis. Reductive decolorization was found to be co-metabolic and mainly associated with hydrogen-producing pathways. We also found evidence of the involvement of an azoreductase from *Lactococcus lactis*. Bacterial community in R1 was sensitive and shifted in the presence of the azo dye, while microorganisms in R2 were more protected. Higher diversity of syntrophic-acetate oxidizers, sulfate reducers and methanogens in R2 highlights the role of the 2nd-stage in organic matter and sulfate removals, and these communities might be involved in further transformations of the azo dye reduction products. The results improve our understanding on the role of different microbial communities in anaerobic treatment of azo dyes and can help in the design of better solutions for the treatment of textile effluents.

* Corresponding author.
E-mail address: jln@bio.aau.dk (J.L. Nielsen).

https://doi.org/10.1016/j.chemosphere.2022.136731
Received 28 April 2022; Received in revised form 10 August 2022; Accepted 1 October 2022
Available online 6 October 2022
0045-6535/© 2022 The Authors. Published by Elsevier Ltd. This is an open access article under the CC BY license (http://creativecommons.org/licenses/by/4.0/).

1. Introduction

Use of multiple stage anaerobic systems can improve reductive decolorization of azo dyes by channeling electrons to preferentially reduce azo bonds in the 1st-stage of the anaerobic digestion (AD), whereas organic matter and sulfate removals are achieved in the following unit with enhanced performance (Oliveira et al., 2022). In this system's configuration, it is expected that distinct microbial communities will stablish in each stage as a result of the different operating conditions applied (Baldi et al., 2019; Demirel and Yenigün, 2002). Acidogens, acetogens and methanogens grow at their optimal ecophysiological conditions, resulting in a better overall process stability compared to single stage anaerobic treatment (García-Depraect et al., 2022). Understanding the role of these microbial communities on the biodegradation of azo dyes can help in the designing of better solutions for the treatment of textile wastewaters.

The conversion of carbohydrates into organic acids occurs in the earliest stage of AD in reactions carried by acidogenic bacteria (Cohen et al., 1980; García-Depraect et al., 2022). In the following step, acetogens and methanogens form syntrophic associations to produce methane (Stams and Plugge, 2009). Under specific conditions, aceticlastic methanogens are inhibited and the Wood–Ljungdahl pathway is inversed (Müller et al., 2013). This rather results in formation of H_2+CO_2 from acetate by the syntrophic acetate oxidizing bacterial (SAOB) community. All these communities are possibly involved in reductive decolorization of azo dyes to a greater or lesser extent.

Some microbial populations play a controversial role in anaerobic treatment of azo dyes. Sulfate-reducing bacterial (SRB) community was found to compete for electrons with azo reducers (Oliveira et al., 2022; Santos et al., 2007), sometimes impairing the reductive decolorization process (Amaral et al., 2014). Nevertheless, decolorization coupled to sulfate reduction was observed before (Albuquerque et al., 2005) and biogenic sulfide can chemically reduce the azo bonds (Prato-Garcia et al., 2013; Zeng et al., 2021). It was hypothesized that whether SRB populations act opposing or in favor of reductive decolorization rather depends on the microbial interspecies interactions and on the biochemical reactions that they are mediating in the system.

Moreover, it is not clear whether mixed microbial cultures rely on specialized enzymes for biodegrading azo dyes. More than a decade ago, Santos et al. (2007) stated that the main mechanism is likely a co-metabolic reaction in which reducing equivalents, as well as reduced cofactors, work as secondary electron donors to cleave the azo bonds. By that time, there were evidence of azoreductases among aerobic bacteria, but no proof in anaerobic microorganisms (Santos et al., 2007; Stolz, 2001). Later on, Morrison et al. (2012) isolated and characterized an anaerobic azoreductase from *Clostridium perfringens*. Decolorization of azo dyes by other enzymes from the oxidoreductase enzyme system, including laccases, NADH–DCIP reductases, veratryl alcohol oxidases, tyrosinases, riboflavin reductases, and lignin and manganese peroxidases was recently reported among pure and co-cultures of microorganisms (Ali et al., 2020; Kurade et al., 2017; Saratale et al., 2013; Waghmode et al., 2011, 2019). Additionally, synergistic action of different oxidoreductase enzymes was proved to enhance decolorization efficiency (Mendes et al., 2011), suggesting that many microbial communities degrade azo dyes through distinct metabolic routes.

This study proposes to bridge the gap between the microbial communities involved in the decolorization of azo dyes in anaerobic treatment systems and the underlying mechanism. The overall bacterial, SAOB, methanogenic, SRB communities were monitored using amplicon sequencing of the 16 S rRNA and functional genes. Efficiency parameters were correlated with the production of volatile fatty acids (VFAs) and metabolites in the system to elucidate the main pathways involved. Sulfidogenic conditions were further applied because sulfate is a common constituent of textile wastewater (Amaral et al., 2014). We provide valuable insights into the anaerobic treatment of azo dyes that can help to better understand how syntrophic microbial communities degrade azo dyes.

2. Materials and methods

2.1. Reactor setup and operational strategies

Two anaerobic reactors were operated continuously over a period of 328 days. The two-phase anaerobic digestion system was composed of a 1st-stage anaerobic structured-bed reactor (R1) and a 2nd-stage upflow anaerobic sludge blanket reactor (R2) running in series and under mesophilic conditions (30 °C). In R1, the fixed-bed was built with polyurethane foam strips (10 × 10 × 650 mm). R1 was operated with a theoretical chemical oxygen demand (COD) of 28.7 gCOD•d^{-1} (organic loading rate = 11.7 gCOD•L^{-1}•d^{-1}) and R2 was operated with 2.7 gCOD•d^{-1} (organic loading rate = 2.0 gCOD•L^{-1}•d^{-1}). Respective hydraulic retention times were 3.5 and 16 h.

R1 was fed with synthetic textile wastewater composed of: Direct Black 22, DB22 (0–65 mg L^{-1}), glucose (1.70 gCOD•L^{-1}), KH_2PO_4 (0.25 g L^{-1}), Na_2SO_4 (0–0.50 g L^{-1}), NaCl (0.50 g L^{-1}), yeast extract (0.20 g L^{-1}), $NaHCO_3$ (0.15 g•g^{-}1•COD) and 1 mL L^{-1} trace elements solution (supplementary material). The pH of the feed was kept at 7.0 ± 0.1. R2 was fed with the effluent from R1 after the addition of $NaHCO_3$ (0.70 g L^{-1}) to raise pH to 6.0. Bioreactors were inoculated with anaerobic sludge from a full scale upflow anaerobic sludge blanket reactor, located in the city of Pereira – SP, processing wastewater from a poultry slaughterhouse. For R1, methanogenic archaea were inactivated by heat-treating the sludge (100 °C, 1 h) previously to inoculation (Wang and Yin, 2017).

Strategies used in the operation of the AD system were as following: startup and stabilization period with no addition of DB22 or SO_4^{2-} (Phase PI); addition of 32.5 mg•L^{-1} DB22 (Phase PII); addition of both 32.5 mg•L^{-1} DB22 and 338 mg•L^{-1} SO_4^{2-} (Phase PIII); and addition of 65.0 mg•L^{-1} DB22 and 338 mg•L^{-1} SO_4^{2-} (Phase PIV).

2.2. Microbial sampling and DNA extraction

Biofilm from R1 and R2 was sampled at different times of each phase after system's performance was stable. In R1, samples were harvested from the bottom biomass of the polyurethane foam used as support for growth. In R2, samples were collected from the sludge blanket (lower portion). Genomic DNA was extracted using the FastDNA® Spin Kit for Soil (MP Biomedicals, Santa Ana, USA) and following the manufacturer's protocols. DNA quantification was assessed using the Quant-iT™ High-Sensitivity DNA Assay Kit on a plate reader (TECAN Infinite M1000) and integrity was evaluated using the TapeStation 2200 with genomic DNA ScreenTapes (Agilent, USA).

2.3. Amplicon sequencing

PCR reactions targeting the V4 variable region of the bacterial 16 S rRNA gene and the functional genes formyltetrahydrofolate synthetase (*fhs*), dissimilatory sulfite reductase β-subunit (*dsrB*), and methyl coenzyme-M reductase (*mcrA*) were further conducted to investigate the SAOB, SRB and methanogenic communities, respectively. Corresponding primer sets are shown in the supplementary materials section. Thermocycler settings were as following: initial denaturation at 95 °C for 2 min; amplification for 25 cycles at 95 °C for 15 s, 50 °C for 15 s, and 72 °C for 60 s; and a final extension of 5 min at 72 °C. Number of cycles, annealing temperature and extension time were appropriately adjusted according to the target gene, as shown in the supplementary materials. Sample preparation was conducted similarly to that described elsewhere (Agneessens et al., 2017), except that for *fhs* a 200 ng of extracted DNA was used as template.

2.4. Bioinformatics processing and statistical analysis

Bioinformatic processing was conducted using the AmpProc 5.1 pipeline (https://github.com/eyashiro/AmpProc), based on USEARCH11 (Edgar, 2013) and QIIME 1.9.1 (Caporaso et al., 2010). For 16 S rRNA gene, *fhs* and *dsrB* amplicons, taxonomy was assigned using MiDAS 4.8.1 (Dueholm et al., 2021), AcetoBase (Singh et al., 2019) and a database of *dsrAB* sequences (Müller et al., 2015). For *mcrA*, a custom database of representative reference sequences was obtained from the Functional Gene Repository (FunGene; http://fungene.cme.msu.edu/). Statistical analysis were performed in R version 4.0.1 via RStudio version 2021.09.0 (http://www.rstudio.com) using the R CRAN package ampvis (v2.7.11) (Albertsen et al., 2015). Structure and differences between microbial communities were assessed using heatmaps and non-metric multidimensional scaling (NMDS) analysis. Sequences were deposited in the European Nucleotide Archive (ENA) database under accession number PRJEB52299.

2.5. Analytical methods and performance evaluation

COD, pH and standard reduction potential (E_0') were measured according to APHA (2005). Sulfide interference on COD analysis was previously eliminated with zinc sulfate addition. For color analysis, samples were appropriately diluted with phosphate buffer (10.86 g L^{-1} NaH_2PO_4 and 5.98 g L^{-1} Na_2HPO_4) (Firmino et al., 2010) and assessed according to the spectra record method (Wu et al., 1998; APHA, 2005). Soluble carbohydrates (CH) and lactic acid were determined as previously described (DuBois et al., 1956; Taylor, 1996). For E_0' profiling in R1, samples were collected at different heights (155, 305, 455, 630 and 750 mm) with the aid of a syringe and transferred to vacuum blood collection tubes. Samples were handled in an anaerobic chamber with N_2 atmosphere. VFAs (C2–C6) and solvents were analyzed by gas chromatography (Adorno et al., 2014).

COD removal (in %) and conversion of CH (CH%, in %) were calculated using Eq. (1).

$$X\ (\%) = \frac{(X_{feed} - X_{effl})}{X_{feed}} \bullet 100 \quad (Eq.\ 1)$$

in which X is either COD removal or CH conversion, X_{feed} is the concentration of X in the feed, and X_{effl} is the concentration of X in the effluent.

Decolorization (in %) was calculated using Eq. (2):

$$Decolorization = \frac{\int_{400\ nm}^{700\ nm} A_{feed} \bullet d\lambda - \int_{400\ nm}^{700\ nm} A_{effl} \bullet d\lambda}{\int_{400\ nm}^{700\ nm} A_{feed} \bullet d\lambda} \bullet 100 \quad (Eq.2)$$

in which A_{feed} is the absorbance of the feed; A_{effl} is the absorbance of the effluent; and $d\lambda$ is an infinitesimal wavelength interval.

2.6. Data analysis

Pearson's correlation analyses were performed in R version 4.0.1 via RStudio version 2021.09.0 using the R CRAN package corrplot (https://github.com/taiyun/corrplot). A significance level of $p \leq 0.05$ was used.

3. Results and discussion

3.1. Two-stage AD system's overall performance

The two-stage AD system was operated for 328 days to investigate how the performance was affected by loading of color and exposure to sulfate. In R1, COD removal efficiencies were below 20% during the entire operation (Table 1) and the volumetric methane production rate rarely exceeded 50 $mL \bullet L^{-1} \bullet d^{-1}$. R1 achieved an average decolorization efficiency of 69 ± 13% when a DB22 loading rate of approximately 222 $mg \bullet L^{-1} \bullet d^{-1}$ was applied in phase PII. Although sulfate was added to the feed as from phase PIII (338 $mg \bullet L^{-1} \bullet SO_4^{2-}$), sulfidogenic activity in R1 was minimal (median sulfate removal = 3.5%, interquartile range = 8.3) and did not impair color removal performance. R2 achieved over 97% of COD and almost 100% sulfate removal efficiencies. Mass balance analysis showed that methanogenesis and sulfidogenesis demanded nearly all the electrons in R2, meaning that the use of a two-stage anaerobic system was important to alleviate the demand of both these processes for reducing equivalents in R1, driving electrons preferentially to reduce the azo dye. Further information on the performance of the two-stage AD system, including the mass balance analysis, had been published elsewhere (Oliveira et al., 2022).

3.2. Azo dye decolorization is mediated by electron shuttles

Color removal profiling in R1 was assessed after performance was stable (Fig. 1-A). The highest increment in color removal was observed between the sampling points *a* and *b*, where decolorization increased from 33 to 90% (as compared to the system's influent). Surprisingly, color removal efficiency decreased in samples taken in sampling point *c* (decolorization = 67%), and further fluctuated across the reactor's profile. This suggests that intermediates produced after the cleavage of the azo bonds were reoxidized in particular zones of the reactor, resulting in the formation of newer azo bonds. It is well known that exposure of byproducts from reductive decolorization to atmospheric oxygen causes the formation of color (Menezes et al., 2019; Oliveira et al., 2020), since hydrazine groups and/or azo anion free radicals in the molecules react with oxygen (Zimmermann et al., 1982). However, there are no studies reporting the reoxidation of aromatic amines inside anaerobic digestors themselves, causing cyclic increases and decreases in color removal across the reactor's profile.

Table 1
Overview of the performance of the two-stage AD system treating azo dye and sulfate.

Phase	Description	Operation days	Average decolorization (%)	Average carbohydrates removal (%)	Average COD removal (%)	Average SO_4^{2-} removal (%)	Effluent pH
1st-stage reactor (R1)							
PI	No DB22 or SO_4^{2-}	1–87	–	97.6 ± 2.6	14.9 ± 5.0	–	4.4 ± 0.1
PII	32.5 $mg \bullet L^{-1} \bullet$DB22	88–182	69 ± 13	91.5 ± 9.7	15.3 ± 5.2	–	4.4 ± 0.1
PIII	32.5 $mg \bullet L^{-1} \bullet$DB22 + 338 $mg \bullet L^{-1} \bullet SO_4^{2-}$	183–263	84 ± 5	99.2 ± 0.2	17.5 ± 3.4	7.9 ± 11	4.5 ± 0.5
PIV	65 $mg \bullet L^{-1} \bullet$DB22 + 338 $mg \bullet L^{-1} \bullet SO_4^{2-}$	264–328	67 ± 12	97.6 ± 1.8	18 ± 3.8	8.0 ± 9.0	4.4 ± 0.1
2nd-stage reactor (R2)							
PI	No DB22 or SO_4^{2-}	1–87	–	N/A	99.8 ± 0.5	–	7.7 ± 0.3
PII	32.5 $mg \bullet L^{-1} \bullet$DB22	88–182	89 ± 4	N/A	98.1 ± 0.4	–	7.6 ± 0.2
PIII	32.5 $mg \bullet L^{-1} \bullet$DB22 + 338 $mg \bullet L^{-1} \bullet SO_4^{2-}$	183–263	80 ± 7	N/A	98.5 ± 0.7	94.4 ± 8.6	7.7 ± 0.3
PIV	65 $mg \bullet L^{-1} \bullet$DB22 + 338 $mg \bullet L^{-1} \bullet SO_4^{2-}$	264–328	87 ± 6	N/A	97.4 ± 0.5	99.6 ± 1.3	8.0 ± 0.3

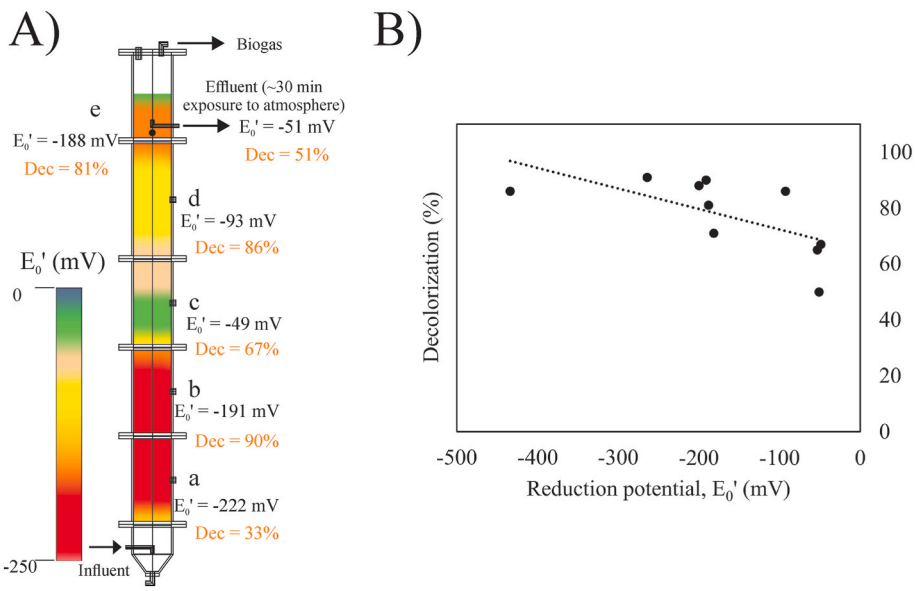

Fig. 1. Association between decolorization efficiency and reduction potential (E_0') in the 1st-stage reactor (R1). **A)** Vertical profiling for decolorization and E_0' in R1; and **B)** Pearson's correlation analysis ($R = -0.64$, $p < 0.05$) for both the variables. Decolorization in each sampling port (a, b, c, d, e and effluent) was calculated relatively to the color of the synthetic wastewater in the feed tank. (For interpretation of the references to color in this figure legend, the reader is referred to the Web version of this article.)

Sampling along R1 further revealed strong zonation with different redox potentials. This reduction potential (E_0') profiling in R1 provided valuable insight into the mechanism of color removal across the 1st-stage reactor's vertical profile. The lower portion of R1, which includes sampling points *a* and *b*, presented more reduced conditions (E_0'~ -200 mV). This is probably because CH conversion reactions into VFAs occurred in the bottom of the reactor (Supplementary material). Moreover, it was previously observed that biohydrogen ($bioH_2$) production from sugars mainly occurs in the basal portion of fixed-bed reactors (Fuess et al., 2021), supporting the hypothesis that the DB22 reduction mechanism is governed by – but not limited to – co-metabolic reactions, in which reducing equivalents or reduced cofactors such as NADH act as secondary electrons donors to cleave azo bonds (Santos et al., 2007).

In the intermediary zone (sampling point *c*), E_0 increased to -49 mV, and DB22 intermediates reoxidized as a result of the less reduced conditions. E_0 values decreased to -93 mV, and further to -188 mV in sampling points *d* and *e*, respectively, causing color removal efficiencies to rise again, oscillating between 81 and 86%. Upon exposure of the effluent to the atmosphere for approximately 30 min, E_0 increased to -51 mV and decolorization decreased to 51%. After repeated measurements were taken across the R1's profile (Fig. 1-B), we confirmed that color removal is negatively correlated with E_0 in system ($R = -0.64$; $p = 0.045$).

The rate of azo reduction has previously been shown to depend on the dye redox potential if the rate-limiting step involves a redox equilibrium between the azo molecule and a reducing agent (Dubin and Wright, 1975). The mechanism hypothesized involves a redox cycle in which a redox mediator transfer electrons between the enzyme and the substrate (Fig. 2). Reduction of the azo dye (R_1-N=N-R_2) to its hydrazo intermediate (R_1-HN–NH–R_2) will only occur if the mediator is present in sufficient concentrations and shifted toward a reduced form (Dubin and Wright, 1975). High concentrations of the reduced mediator will result in decreased E_0 values, and electron transfer to azo compounds will happen once the redox potential in the environment approach that of the dye. However, this last reaction is reversible as long as the hydrazo intermediate is not further degraded. It can be hypothesized that the equilibrium shifted towards re-oxidation of DB22 intermediates (e.g., hydrazo to azo) as reduction potential in the system increased due to consumption of mediators in the reduced form, causing reappearance of color in the upper portion of R1.

3.3. Co-metabolic routes involved in reductive decolorization

Conversion of carbohydrates occurred in R1 with efficiencies of approximately 99% throughout the 328 days of operation. Production of VFAs and metabolites in the effluent after R1 was monitored and is shown in the supplementary materials section.

Butyrate-type fermentation was the main pathway observed during the stabilization phase. Median concentrations of HBu and HAc were, respectively, 295 mg•L^{-1} (interquartile range = 245) and 154 mg•L^{-1} (interquartile range = 220) in this period, which accounts for a HBu/HAc ratio of 1.91. In phases PII and PIII (32.5 mg•L^{-1} DB22), HBu/HAc ratios decreased to 0.79 and 0.98, while HPr concentrations remained similar (PI: median 132 mg•L^{-1}, interquartile range = 117; PII: median 118 mg•L^{-1}, interquartile range = 46; and PIII: median 156 mg•L^{-1},

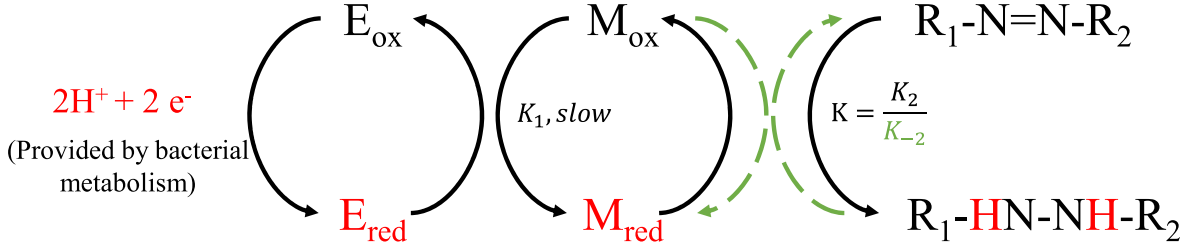

Fig. 2. Postulated mechanism of azo dye decolorization in anaerobic systems by redox mediators. E_{red}/E_{ox} are, respectively, the reduced and oxidized forms of an enzyme, and M_{red}/M_{ox} are the reduced and oxidized forms of a low molecular weight electron carrier (mediator). Green arrows represent a shift in the equilibrium towards reoxidation of the hydrazo intermediate and generation of newer azo bonds. Adapted from Dubin and Wright (1975). (For interpretation of the references to color in this figure legend, the reader is referred to the Web version of this article.)

interquartile range = 82). These results indicate the predominance of the acetic pathway (Table 2, Eq. 2) during most of the operation with the azo dye, which is usually associated with higher bioH_2 production rates from CH when compared to other more reduced metabolites (Fernandes et al., 2010; Fuess et al., 2016).

The involvement of the acetic fermentation pathway on reductive decolorization is further supported by results from Pearson's correlation test ($R = 0.48$, $p = 0.001$) performed with samples collected all over the operation (Fig. 3-A). Butyrate fermentation (Table 2, Eq. 3), another hydrogen-producing reaction, was also significant for color removal ($R = 0.35$, $p = 0.021$). Since bioH_2 was not released in the biogas phase (Oliveira et al., 2022), some of the reducing power generated via these metabolic routes might have been consumed during co-metabolic decolorization of DB22.

The strongest correlation was found to be between decolorization and CH% ($R = 0.60$, $p < 0.001$). In fact, the catabolism of glucose to pyruvate yields two NADH molecules (Table 2, Eq. 1), which can serve as reducing power for the cleavage of azo bonds. Moreover, glycolysis is the precursor of all mixed acid fermentation reactions and acidogenesis was found to be a critical step in AD of azo dyes (Firmino et al., 2010; Li et al., 2014).

Interestingly, metabolites produced via hydrogen-consuming reactions such as n-valeric acid (Table 2, Eq. 9), ethanol (Table 2, Eq. 10) and methanol (Table 2, Eq. 11) were also positively correlated with color removal. For instance, n-valerate elongation from propionate consumes six mols of H_2. Both ethanol and methanol formation obtain reducing power from NADH+H^+. Nevertheless, the correlations between these metabolites and reductive decolorization may reflect the fermentative diversity in R1 rather than causation directly. Several studies have shown the benefits of metabolic diversity on decolorization of azo dyes by mixed microbial cultures due to the synergistic action of different enzymes from the oxidoreductase system. Observed increases in the activities of NADH-DCIP reductases, azoreductases, veratryl alcohol oxidases and laccases after decolorization of textile effluents by microbial consortiums rather than in controls with the respective individual isolates were previously observed (Kurade et al., 2017; Phugare et al., 2011). In another study, decolorization was found to be correlated with higher microbial diversity in batch experiments, further supporting the relevance of metabolic diversity in the biodegradation of azo dyes (Oliveira et al., 2020). Finally, production and accumulation of metabolites such as ethanol may stimulate other hydrogen-producing routes, e.g., chain elongation to n-caproic acid production (Cavalcante et al., 2017), therefore explaining the positive correlation between ethanol and decolorization.

Table 2
Main fermentation pathways involved in co-metabolic decolorization of the azo dye Direct Black 22. Adapted from Cavalcante et al. (2017); Mariano et al. (2011); Saady (2013); and Xin et al. (2004).

Pathway	Reaction	No.
I - Hydrogen-producing reactions (as H_2 or NADH+H^+)		
Glucose to pyruvate formation	Glucose → 2pyruvate + 2 NADH+H^+	(1)
Glucose to acetic acid formation	Glucose + $2H_2O$ → 2acetic acid + $4H_2$ + $2CO_2$	(2)
Glucose to butyric acid formation	Glucose → butyric acid + $2H_2$ + $2CO_2$	(3)
Ethanol to n-caproic acid generation	12ethanol + 3acetic acid → 5n-caproic acid + $4H_2$ + $8H_2O$	(4)
Lactic acid to n-caproic acid generation	15lactic acid → 5n-caproic acid + $5CO_2$ + $10H_2$ + $5H_2O$	(5)
Glucose to acetone formation	Glucose + $2H_2O$ → 1acetone + $4H_2$ + $3CO_2$	(6)
n-Butyric acid oxidation	n-Butyric acid + $2H_2O$ → 2acetic acid + $2H_2$	(7)
II - Hydrogen-consuming reactions (as H_2 or NADH+H^+)		
Pyruvate to acid lactic formation	Pyruvate + NADH+H^+ → Lactic acid + NAD^+	(8)
Propionic acid to n-valeric acid elongation	Propionic acid + $2CO_2$ + $6H_2$ → n-valeric acid + $4H_2O$	(9)
Glucose to ethanol formation[a]	Glucose → 2ethanol + $2CO_2$	(10)
Methane to methanol formation	CH_4 + ½O_2 + NADH+H^+ → Methanol + NAD^+	(11)

[a] No net hydrogen production/consumption.

Pearson's correlation analysis was also performed separately for each system's operational strategy. In phase PII (32.5 mg•L^{-1} DB22), decolorization was significantly correlated with CH% and the production of HBu, HVa, HCa and ethanol (Fig. 3-B). Production of n-caproic acid from both ethanol and lactic acid yields bioH_2 that can be used as reducing power for reductive decolorization (Table 2, Eq. 4-5). Ethanol elongation to n-caproic acid likely occurred because both ethanol and acetic acid were present in phase PII, and ethanol concentrations were strongly correlated with those of n-caproic acid ($R = 0.55$, $p = 0.040$). Moreover, lactic acid was detected in samples collected all over PII operation at concentrations ranging from 10 to 32 mg L^{-1}. Given the high abundance of homolactic bacteria in R1 (see Topic 3.6), lactic acid was probably utilized to generate n-caproic acid. It can therefore be hypothesized that decolorization of DB22, in phase PII, was mainly driven by reactions involved in chain elongation for n-caproate production.

Addition of sulfate (338 mg L^{-1} SO_4^{2-}), in phase PIII, did not appear to affect decolorization and CH% efficiencies in R1 (Fig. 3-C). Effluent sulfate concentrations remained similar and, sometimes, slightly higher than those measured in the feed tank. In fact, the 1st-stage reactor was designed with the aim of preventing sulfidogenesis, thus avoiding competition between the azo dye and sulfate for reducing equivalents. Although no sulfate removal occurred in R1, Pearson's correlation analysis results showed that distinct metabolic routes were involved in DB22 decolorization in phase PIII. Decolorization was positively correlated with acetone formation ($R = 0.57$, $p = 0.018$), which is a bioH_2 producing reaction (Table 2, Eq. 6), and negatively associated with HBu concentration ($R = -0.51$, $p = 0.035$) in this period. The later suggests that the decrease in HBu/HAc ratio occurred as a result of butyrate oxidation (Table 2, Eq. 7), which leads do the production of bioH_2 that can serve as additional electron donor for reductive decolorization. The findings agree with previous studies in which the presence of an azo dye led to higher decomposition of VFAs (propionate and butyrate) into acetate, compared to a control without azo dye (Li et al., 2014). The authors hypothesized that bioH_2 produced in acetification of VFAs served as additional reducing power for reductive decolorization. This was further supported by results from enzymatic assays, which showed that azoreductase activity was higher in the presence of butyrate and propionate than acetate.

After applied DB22 loading rate was increased to 438 ± 13 mg•L^{-1}•d^{-1} (65 mg•L^{-1}, Phase PIV), we observed a lower metabolic diversity in R1 (Fig. 3-D). Methanol, ethanol and acetone were not detected as from the 5th day after transition to phase PIV, and HBu/HAc ratio increased to 1.70. Moreover, no correlations were found between the produced metabolites and decolorization. This period of operation was marked by a decrease in decolorization efficiencies in R1, with later stabilization at lower removal rates. This further supports our hypothesis that a higher metabolic diversity is beneficial for reductive decolorization of azo dyes.

3.4. Overall bacterial community and sensitivity of acidogens towards azo dye

After a DB22 loading rate of 222 ± 9 mg•L^{-1}•d^{-1} (32.5 mg•L^{-1}, Phase PII) was applied to R1, CH% had a sudden drop from approximately 99 to 70%, with gradual recovery in the following weeks (Oliveira et al., 2022). This suggests that microorganisms adapted to the dye and to intermediates of the reductive decolorization. However, this could also mean that a microbial community with different structure was stablished in the system. Molecular identification of microorganisms based on the 16 S rRNA and functional genes was further conducted to understand the possible causes.

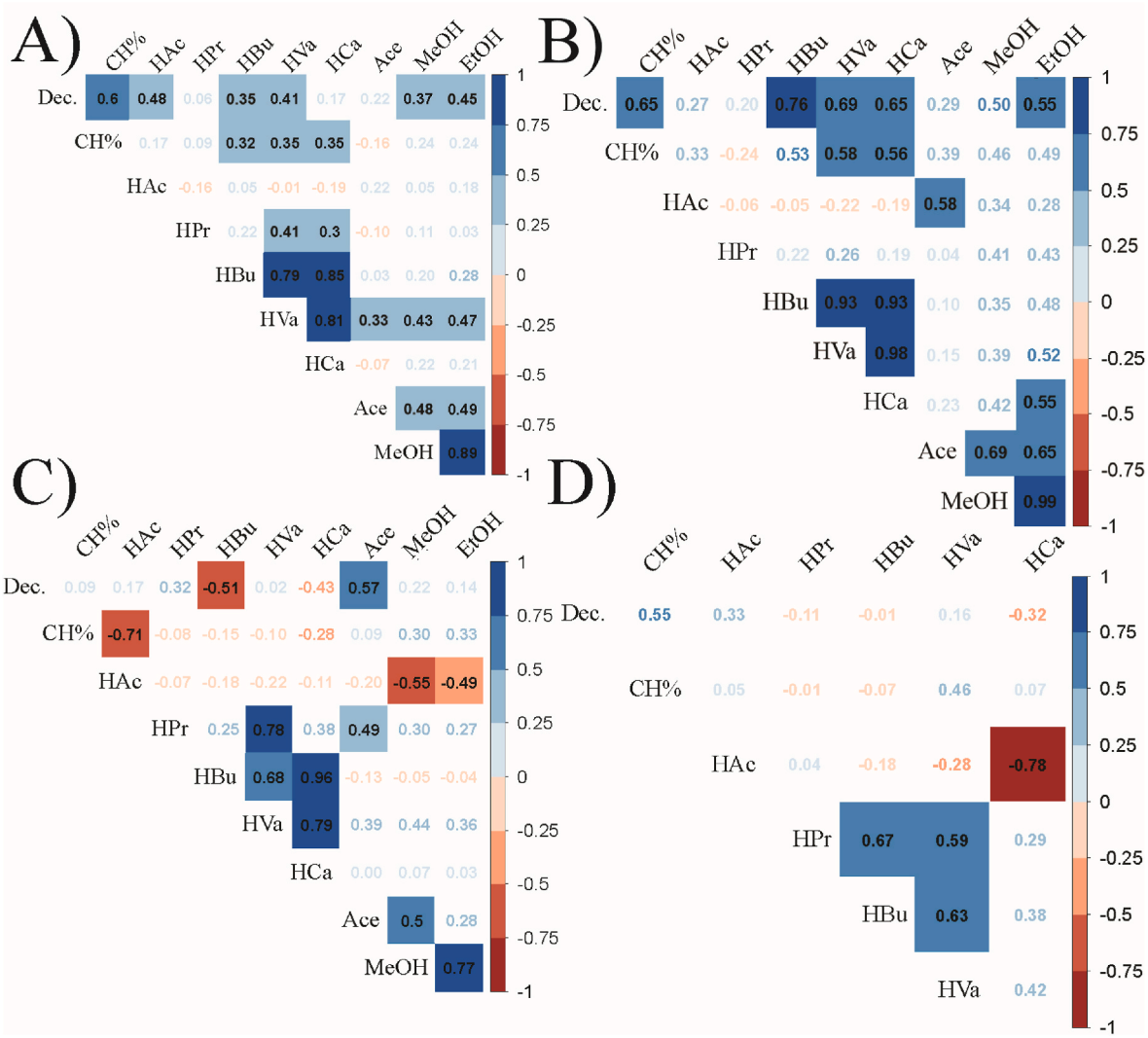

Fig. 3. Pearson's correlation matrix (significance level $p \leq 0.05$) for DB22 decolorization (Dec, in %), carbohydrates conversion efficiency (CH%, in %), volatile organics acids (acetic acid – HAc, propionic acid – HPr, n-butyric acid – HBu, n-valeric acid – HVa, n-caproic acid – HCa, in mg•L^{-1}) and metabolites (methanol – MeOH, ethanol – EtOH, acetone – Ace, in mg·L^{-1}). **A)** All operational phases, n = 43 obs.; **B)** PII: 32.5 mg•L^{-1} DB22, n = 14 obs..; **C)** PIII: 32.5 mg•L^{-1} DB22 and 338 mg•L^{-1} SO_4^{2-}, n = 17 obs.; and **D)** PIV: 65 mg•L^{-1} DB22 and 338 mg•L^{-1} SO_4^{2-}, n = 12 obs.

Amplicon sequencing of the 16 S rRNA gene targeting the V4 region revealed a significant shift in the bacterial community structure in R1 after DB22 was added to the system, in phase PII (Fig. 4-A). Samples clustered into four groups, of which each one represented a different operational strategy. DB22 was found to be the main source of variation in the dataset, since samples from phase PI (operation without the azo dye) clustered separately on the left side of NMDS1 axis, apart from the other phases, which grouped to the right side. Within this main group, samples from phase PII (operation with no sulfate addition) clustered in the upper-right quadrant, while samples from phases PIII and PIV (338 mg•L^{-1} SO_4^{2-} added to the feed) grouped in the lower-right portion. These results indicate that sulfate is the second largest source of variation in the gradient analysis. Calculated stress-value was 0.05, which suggests a relative strong separation of the microbial communities (Paliy and Shankar, 2016).

Some members of the family *Clostridiaceae* and of the genera *Lactococcus*, *Prevotella* and *Atopobium* increased in proportion in the presence of the azo dye, while members of *Ruminococcaceae* and *Clostridium sensu stricto 1* were negatively affected. Members of Firmicutes predominated in all conditions, with relative abundance values of 66–80% (PI), 53–67% (PII), 72–76% (PIII) and 76–81% (PIV) (Supplementary materials). This phylum is often favored under acidogenic conditions (Ribeiro et al., 2022) and was recently associated with azo-reducing activity in the gut microbiota (Zahran et al., 2021).

Fig. 5-A shows the most abundant genera in R1 as a function of operational phase. *Lactococcus*, an homolactic bacteria belonging to Firmicutes, increased in proportion from 0.9 to 9.2% (PI) to 16.9%, in PII, and up to 26.7% after DB22 loading rate was further increased (PIV). In a study conducted by Pérez-Díaz and McFeeters (2009), several lactic acid bacteria were able to modify an azo dye under anaerobic and even aerobic conditions, and therefore *Lactococcus* is a potential azo degrader.

Clostridium was also positively selected in the presence of the azo dye, accounting for 19.5% of the overall bacterial community in the end of the operation (day 328). An anaerobic azoreductase capable of reducing high molecular weight sulfonated azo dyes has been recently described in a member of *Clostridium* (Morrison and John, 2015), meaning that this bacterium might be involved in the biodegradation of DB22.

Prevotella and *Atopobium*, which have no previous records regarding azo decolorization, were also among the genera that were positively selected in the presence of DB22. *Prevotella* can produce acetate from glucose (Takahashi and Yamada, 2000) and major end-products of *Atopobium* include lactic acid and acetate (Acevedo Monroy and Kizilova, 2006; Burton et al., 2004). Since acetate formation presented a

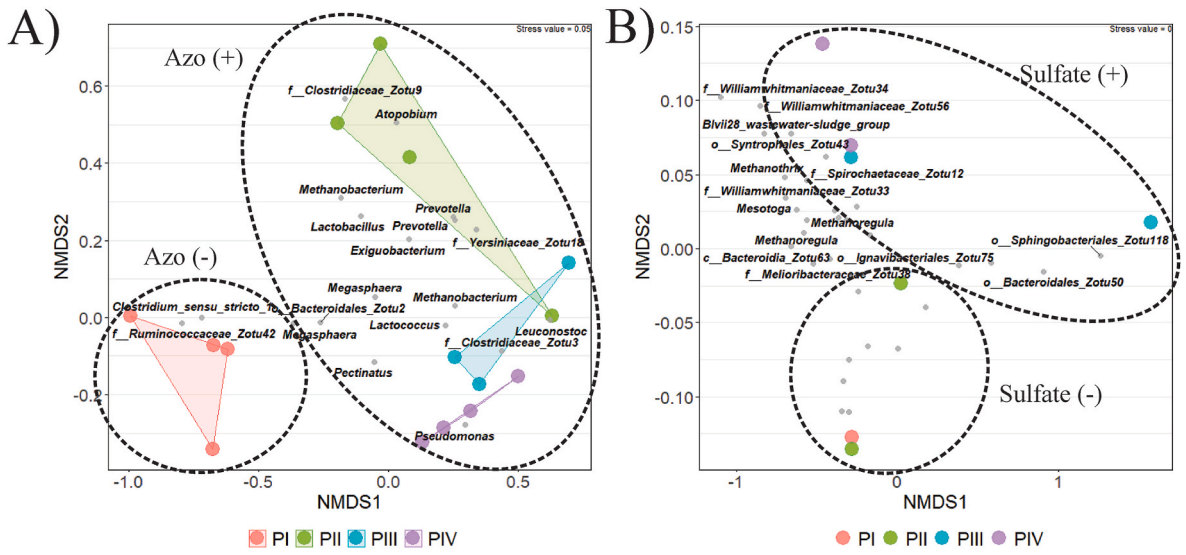

Fig. 4. Non-metric multidimensional scaling (NMDS) analysis based on Bray-Curtis distance for the overall bacterial community in the **A)** 1st-stage (R1) and **B)** 2nd-stage (R2) reactors. Low abundant amplicon sequencing variants (ASVs) were removed from the analysis using a 1.5% threshold.

strong correlation with color removal (Section 3.3), these bacteria could be involved in decolorization of DB22 via inter-species hydrogen transfer.

On the contrary, samples from R2 rather grouped by either the absence (PI and PII) or presence (PIII and PIV) of sulfate ions in the feed (Fig. 4-B), suggesting that azo dyes and/or intermediates from reductive decolorization had little impact on the bacterial community structure in R2. This is likely because microorganisms in R2 were less exposed to the dye, since most of the decolorization occurred in R1, which also received a higher DB22 load. Nevertheless, these microorganisms were still exposed to aromatic amines and other DB22 fragments recalcitrant to the AD.

Syntrophobacter and *Desulfovibrio* were among the genera that were enriched in the presence of sulfate. *Syntrophobacter* increased in proportion from 0.7 to 1%, in phase PII, to 2.5–5.8% after sulfate was introduced into the system (Fig. 5-B). *Desulfovibrio* increased its relative abundance from 0.5 to 1.6 to up to 2.6% under the same conditions. Both are sulfate reducers with fermentation ability (Muyzer and Stams, 2008). SRB community in the two-stage AD system will be covered with more detail in the next section.

3.5. Sulfate reducing bacterial (SRB) and methanogenic communities in the two-stage AD system

No sequences of the *dsrB* and few sequences of the *mcrA* genes were obtained in samples from R1. Indeed, SRB and methanogens were not expected in this reactor due the low pH (pH 4.3–4.5). In R2, methanogenic community presented minor variations during the system's operation (supplementary materials). Uncultured *Methanobacteriales archaeon*, *Methanosaeta concilii GP-6*, and *Methanosaeta concilii* were the only taxa enriched in the presence of DB22 (Phases PII, PIII and PIV). Members of the order *Methanobacteriales* generally use H_2 + CO_2 to produce methane (Acevedo Monroy and Kizilova, 2006), therefore uncultured *Methanobacteriales archaeon* is likely to compete with azo reducers, especially since it accounted for nearly 50% of the methanogenic community in R2. *Methanosaeta concilii*, which comprised up to 20.6% of the *mcrA* sequences in phase PIV, is the only methanogen in R2 capable of utilizing acetate as substrate for methanogenesis (Barber et al., 2011). The increased proportion of hydrogenotrophic methanogens shows that production of methane derived primarily from hydrogen and carbon dioxide, but competition between azo reducers and hydrogen-utilizing methanogens was minimized because bulk color removal occurred in the preceding unit, i.e. R1.

It is important to point out that R2 was inoculated with sludge from a UASB reactor processing wastewater from a poultry slaughterhouse, which are enriched with hydrogenotrophic methanogens. Ammonia released in the biodegradation of protein-rich effluents leads to inhibition of aceticlastic methanogens and in inversion of the Wood–Ljungdahl pathway by SAOB community (Müller et al., 2013). DB22 biodegradation may result in increasing concentrations of ammonia as well. Both the source of the inoculum and the presence of DB22 might have influenced the predominance of hydrogen-utilizing methanogens.

SRB community structure in samples from phases PIII and PIV – which correspond to the operation with added sulfate – did not present a significant shift after the increment in DB22 loading rate (supplementary materials). Although *Desulfobulbus propionicus* demonstrated a large increase in proportion in phase PIV (approximately 52%), this enrichment had started in the previous phase, at lower concentrations of the azo dye. *Desulfobulbus propionicus* is capable of oxidizing propionate in the presence of sulfate, sulfite or thiosulfate as terminal electron acceptors (Widdel and Pfennig, 1982). Sulfide produced (Reaction 1) can be involved in further transformation of DB22 reduction products in R2, as well as in additional removal of color, since an increase in the concentration of total aromatic amines was observed in this reactor (Oliveira et al., 2022). This is because chemical reduction of azo bonds by sulfide can be expected under sulfidogenic conditions, but the contribution of this mechanism was found to be little compared to biological reduction (Van Der Zee et al., 2003). Propionate oxidation leads to formation of acetate (Reaction 1), and therefore *D. propionicus* can establish syntrophic interactions with *Methanosaeta concilii* instead of competing for acetate.

$$4propionate^- + 3SO_4^{2-} \rightarrow 4acetate^- + 4HCO_3^- + 3HS^- + H^+ \quad (Reaction\ 1)$$

3.6. Syntrophic acetate-oxidizing bacterial (SAOB) and acetogenic communities in the two-stage AD system

Amplicon sequencing targeting the *fhs* gene was conducted in samples from the two-stage AD system to investigate the SAOB and acetogenic communities. A low diversity of these populations was observed in R1, where *Leuconostoc mesenteroides* predominated in all operational phases (62–95%), regardless of the presence of DB22 or sulfate (supplementary materials). *L. mesenteroides* is an heterolactic lactic acid bacterium (LAB) that produces lactic acid, ethanol and/or acetate as

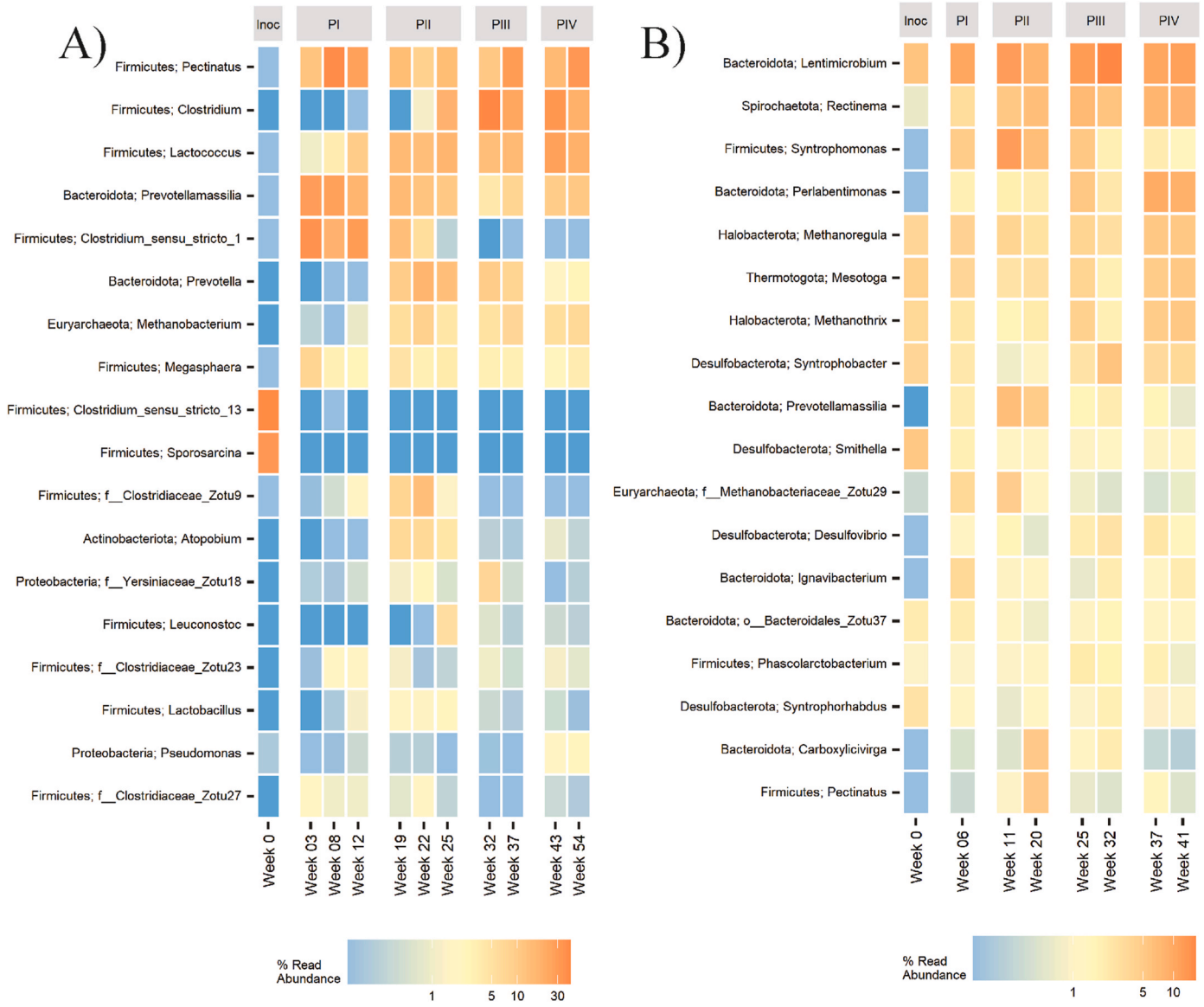

Fig. 5. Heatmap of the top 18 amplicon sequencing variants (ASVs) in the **A)** 1st-stage (R1) and **B)** 2nd-stage (R2) reactors identified after targeting the bacterial *16S rRNA* V4 region. Samples are faceted by the operational strategies used in the operation of the AD system.

main fermentation end-products (Özcan et al., 2019).

On the other hand, the homolactic LAB *Lactococcus lactis* was clearly selected in the presence of the azo dye, increasing its relative abundance from 0 to 2.4% in the stabilization phase to up to 11.5% at 32.5 mg•L^{-1} DB22 (Phases PII and PIII), and further to 16.1% when DB22 concentration was further increased to 65 mg•L^{-1} DB22 (Phase PIV). These results are compatible with those from the 16 S rRNA gene amplicon sequencing analysis (Section 3.4) and suggests that *L. lactis* is involved in reductive decolorization of DB22 through the pathway in Eq. 8 (Table 2). However, it is not clear whether decolorization mediated by *L. lactis* is a typical co-metabolic reaction carried by redox mediators. $NADH+H^+$ produced in glycolysis is recycled during lactate formation from pyruvate, resulting in no net hydrogen production. Other studies reported azo dye reduction by *L. lactis* (You and Teng, 2009) and LAB (Pérez-Díaz and McFeeters, 2009). We hypothesize that azo dye decolorization by *L. lactis* occurs through the action of enzymes with high specificity to azo dyes, since genes encoding the production of the enzyme FMN-dependent NADH-azoreductase were found in the genome of *L. lactis* isolated from this same reactor (unpublished data).

SAOB and acetogenic communities were more diverse in R2 (supplementary materials). *Prevotella melaninogenica* was remarkably enriched at higher DB22 concentrations (Phase PIV), accounting for up to 41.1% of the *fhs* sequences. This bacterium is able to produce acetic and succinic acids as primary end products of glucose or lactose fermentation (Shah and Gharbia, 1992). On the other hand, *Sporolituus thermophilus* (Ogg and Patel, 2009), which utilizes both malate and citrate, decreased in proportion throughout R2 operation, particularly under sulfidogenic conditions (Phases PIII and PIV). Probably, this apparent drop in the relative abundance is rather a consequence of the enrichment of *P. melaninogenica*.

Brachybacterium phenoliresistens presented an increasing pattern in its relative abundance values as from phase PIII, i.e. after sulfate addition. This specie can degrade hydrocarbons under high salinity conditions and have been isolated from oil-contaminated sites (Chou et al., 2007; Wang et al., 2014). The ability to survive in saline environments explain the enrichment of this bacterium after exposure to sulfate. Moreover, the proportion of *B. phenoliresistens* further increased to 12.4% when higher DB22 concentrations were loaded into the system, which can be attributed to the ability of this species to tolerate high levels of phenol and degrade hydrocarbons. DB22 was converted to aromatic compounds

in the preceding unit, which could not be further mineralized, but were transformed in R2 (Oliveira et al., 2022). This means that *B. phenoliresistens* could be involved in the transformation of hydrocarbons in R2.

4. Conclusion

Azo dye decolorization in the two-stage AD system occurs mainly as a result of hydrogen-producing reactions (in the form of H_2 and/or reduced cofactors) in a mechanism mediated by electron shuttles. Enzymes with high specificity (e.g. azoreductases from *L. lactis*) seems to play an important role as well. Acidogens from R1 were observed to be sensitive and undergo selection upon exposure to azo dyes, whereas microbial communities in R2 are exposed to lower levels of azo dye and therefore appear less sensitive. These results are relevant when considering organic matter and sulfate removals and biogas production in R2, as methanogens and SRB show less impact under these circumstances.

Credit author statement

Jean M. S. Oliveira: Conceptualization, Investigation, Writing-Original draft preparation. **Jan S. Poulsen:** Methodology, Software, Data Curation, Writing - Review & Editing. **Eugênio Foresti**: Conceptualization, Resources, Supervision. **Jeppe L. Nielsen:** Conceptualization, Resources, Supervision, Writing - Review & Editing.

Declaration of competing interest

The authors declare that they have no known competing financial interests or personal relationships that could have appeared to influence the work reported in this paper.

Data availability

Data will be made available on request.

Acknowledgement

This work was supported by Aalborg University, the Fundação do Amparo à Pesquisa do Estado de São Paulo (process numbers 2015/06246-7, 2018/24269-2 and 2020/11860-4), and the Coordenação de Aperfeiçoamento de Pessoal de Nível Superior (CAPES) – Brazil (Finance Code001). The authors also would like to thank Dr. Nadieh de Jonge for her technical support.

Appendix A. Supplementary data

Supplementary data to this article can be found online at https://doi.org/10.1016/j.chemosphere.2022.136731.

References

Acevedo Monroy, S.E., Kizilova, A., 2006. The Prokaryotes. Springer, New York, NY. https://doi.org/10.1007/0-387-30743-5. New York.

Adorno, M.A.T., Hirasawa, J.S., Varesche, M.B.A., 2014. Development and validation of two methods to quantify volatile acids (C2-C6) by GC/FID: headspace (automatic and manual) and liquid-liquid extraction (LLE). Am. J. Anal. Chem. 406–414. https://doi.org/10.4236/ajac.2014.57049, 05.

Agneessens, L.M., Ottosen, L.D.M., Voigt, N.V., Nielsen, J.L., de Jonge, N., Fischer, C.H., Kofoed, M.V.W., 2017. In-situ biogas upgrading with pulse H2 additions: the relevance of methanogen adaption and inorganic carbon level. Bioresour. Technol. 233, 256–263. https://doi.org/10.1016/j.biortech.2017.02.016.

Albertsen, M., Karst, S.M., Ziegler, A.S., Kirkegaard, R.H., Nielsen, P.H., 2015. Back to basics - the influence of DNA extraction and primer choice on phylogenetic analysis of activated sludge communities. PLoS One 10, 1–15. https://doi.org/10.1371/journal.pone.0132783.

Albuquerque, M.G.E., Lopes, A.T., Serralheiro, M.L., Novais, J.M., Pinheiro, H.M., 2005. Biological sulphate reduction and redox mediator effects on azo dye decolourisation in anaerobic-aerobic sequencing batch reactors. Enzym. Microb. Technol. 36, 790–799. https://doi.org/10.1016/j.enzmictec.2005.01.005.

Ali, S.S., Al-Tohamy, R., Xie, R., El-Sheekh, M.M., Sun, J., 2020. Construction of a new lipase- and xylanase-producing oleaginous yeast consortium capable of reactive azo dye degradation and detoxification. Bioresour. Technol. 313, 123631 https://doi.org/10.1016/j.biortech.2020.123631.

Amaral, F.M., Kato, M.T., Florêncio, L., Gavazza, S., 2014. Color, organic matter and sulfate removal from textile effluents by anaerobic and aerobic processes. Bioresour. Technol. 163, 364–369. https://doi.org/10.1016/j.biortech.2014.04.026.

APHA, 2005. Standard Methods for the Examination of Water and Wastewater, twentieth ed. American Public Health Association, American Water Works Association, Water Environment Federation. American Public Health Association, American Water Works Association, Water Environment Federation, Washington.

Baldi, F., Pecorini, I., Iannelli, R., 2019. Comparison of single-stage and two-stage anaerobic co-digestion of food waste and activated sludge for hydrogen and methane production. Renew. Energy 143, 1755–1765. https://doi.org/10.1016/j.renene.2019.05.122.

Barber, R.D., Zhang, L., Harnack, M., Olson, M.V., Kaul, R., Ingram-Smith, C., Smith, K. S., 2011. Complete genome sequence of Methanosaeta concilii, a specialist in aceticlastic methanogenesis. J. Bacteriol. 193, 3668–3669. https://doi.org/10.1128/JB.05031-11.

Burton, J.P., Devillard, E., Cadieux, P.A., Hammond, J.A., Reid, G., 2004. Detection of Atopobium vaginae in postmenopausal women by cultivation-independent methods warrants further investigation. J. Clin. Microbiol. 42, 1829–1831. https://doi.org/10.1128/JCM.42.4.1829-1831.2004.

Caporaso, J.G., Kuczynski, J., Stombaugh, J., Bittinger, K., Bushman, F.D., Costello, E.K., Fierer, N., Peña, A.G., Goodrich, J.K., Gordon, J.I., Huttley, G.A., Kelley, S.T., Knights, D., Koenig, J.E., Ley, R.E., Lozupone, C.A., Mcdonald, D., Muegge, B.D., Pirrung, M., Reeder, J., Sevinsky, J.R., Turnbaugh, P.J., Walters, W.A., Widmann, J., Yatsunenko, T., Zaneveld, J., Knight, R., 2010. QIIME allows analysis of high-throughput community sequencing data. Nat. Methods 7, 335–336. https://doi.org/10.1038/nmeth0510-335.

Cavalcante, W. de A., Leitão, R.C., Gehring, T.A., Angenent, L.T., Santaella, S.T., 2017. Anaerobic fermentation for n-caproic acid production: a review. Process Biochem. 54, 106–119. https://doi.org/10.1016/j.procbio.2016.12.024.

Chou, J.H., Lin, K.Y., Lin, M.C., Sheu, S.Y., Wei, Y.H., Arun, A.B., Young, C.C., Chen, W. M., 2007. Brachybacterium phenoliresistens sp. nov., isolated from oil-contaminated coastal sand. Int. J. Syst. Evol. Microbiol. 57, 2674–2679. https://doi.org/10.1099/ijs.0.65019-0.

Cohen, A., Breure, A.M., Andel, J.G.V.A.N., Deursen, A.V.A.N., 1980. Influence of phase separation on the anaerobic digestion of glucose - maximum COD-turnover rate during continuous operation. Water Res. 14, 1439–1448.

Demirel, B., Yenigün, O., 2002. Two-phase anaerobic digestion processes: a review. J. Chem. Technol. Biotechnol. 77, 743–755. https://doi.org/10.1002/jctb.630.

Dubin, P., Wright, K.L., 1975. Reduction of azo food dyes in cultures of proteus vulgaris. Xenobiotica 5, 563–571. https://doi.org/10.3109/00498257509056126.

DuBois, M., Gilles, K.A., Hamilton, J.K., Rebers, P.A., Smith, F., 1956. Colorimetric method for determination of sugars and related substances. Anal. Chem. 28, 350–356. https://doi.org/10.1021/ac60111a017.

Dueholm, M.S., Nierychlo, M., Andersen, K.S., Rudkjøbing, V., Knutsson, S., Consortium, the M.G., Albertsen, M., Nielsen, P.H., 2021. MiDAS 4: A Global Catalogue of Full-Length 16S rRNA Gene Sequences and Taxonomy for Studies of Bacterial Communities in Wastewater Treatment Plants. 10.1101/2021.07.06.451231.

Edgar, R.C., 2013. UPARSE: highly accurate OTU sequences from microbial amplicon reads. Nat. Methods 10, 996–998. https://doi.org/10.1038/nmeth.2604.

Fernandes, B.S., Peixoto, G., Albrecht, F.R., Saavedra del Aguila, N.K., Zaiat, M., 2010. Potential to produce biohydrogen from various wastewaters. Energy Sustain. Dev. 14, 143–148. https://doi.org/10.1016/j.esd.2010.03.004.

Firmino, P.I.M., da Silva, M.E.R., Cervantes, F.J., dos Santos, A.B., 2010. Colour removal of dyes from synthetic and real textile wastewaters in one- and two-stage anaerobic systems. Bioresour. Technol. 101, 7773–7779. https://doi.org/10.1016/j.biortech.2010.05.050.

Fuess, L.T., Fuentes, L., Bovio-Winkler, P., Eng, F., Etchebehere, C., Zaiat, M., Oller do Nascimento, C.A., 2021. Biohydrogen-producing from bottom to top? Quali-quantitative characterization of thermophilic fermentative consortia reveals microbial roles in an upflow fixed-film reactor. Chem. Eng. J. Adv. 7, 100125 https://doi.org/10.1016/j.ceja.2021.100125.

Fuess, L.T., Mazine Kiyuna, L.S., Garcia, M.L., Zaiat, M., 2016. Operational strategies for long-term biohydrogen production from sugarcane stillage in a continuous acidogenic packed-bed reactor. Int. J. Hydrogen Energy 41, 8132–8145. https://doi.org/10.1016/j.ijhydene.2015.10.143.

García-Depraect, O., Martínez-Mendoza, L.J., Diaz, I., Muñoz, R., 2022. Two-stage anaerobic digestion of food waste: enhanced bioenergy production rate by steering lactate-type fermentation during hydrolysis-acidogenesis. Bioresour. Technol. 358, 127358 https://doi.org/10.1016/j.biortech.2022.127358.

Kurade, M.B., Waghmode, T.R., Patil, S.M., Jeon, B.H., Govindwar, S.P., 2017. Monitoring the gradual biodegradation of dyes in a simulated textile effluent and development of a novel triple layered fixed bed reactor using a bacterium-yeast consortium. Chem. Eng. J. 307, 1026–1036. https://doi.org/10.1016/j.cej.2016.09.028.

Li, Y., Zhang, Y., Quan, X., Zhang, J., Chen, S., Afzal, S., 2014. Enhanced anaerobic fermentation with azo dye as electron acceptor: simultaneous acceleration of organics decomposition and azo decolorization. J. Environ. Sci. (China) 26. https://doi.org/10.1016/j.jes.2014.07.009, 1970–1976.

Mariano, A.P., Keshtkar, M.J., Atala, D.I.P., Filho, F.M., MacIel, M.R.W., Filho, R.M.I., Stuart, P., 2011. Energy requirements for butanol recovery using the flash

fermentation technology. Energy Fuel. 25, 2347–2355. https://doi.org/10.1021/ef200279v.
Mendes, S., Farinha, A., Ramos, C.G., Leitão, J.H., Viegas, C.A., Martins, L.O., 2011. Synergistic action of azoreductase and laccase leads to maximal decolourization and detoxification of model dye-containing wastewaters. Bioresour. Technol. 102, 9852–9859. https://doi.org/10.1016/j.biortech.2011.07.108.
Menezes, O., Brito, R., Hallwass, F., Florêncio, L., Kato, M.T., Gavazza, S., 2019. Coupling intermittent micro-aeration to anaerobic digestion improves tetra-azo dye Direct Black 22 treatment in sequencing batch reactors. Chem. Eng. Res. Des. 146, 369–378. https://doi.org/10.1016/j.cherd.2019.04.020.
Morrison, J.M., John, G.H., 2015. Non-classical azoreductase secretion in Clostridium perfringens in response to sulfonated azo dye exposure. Anaerobe 34, 34–43. https://doi.org/10.1016/j.anaerobe.2015.04.007.
Morrison, J.M., Wright, C.M., John, G.H., 2012. Identification, Isolation and characterization of a novel azoreductase from Clostridium perfringens. Anaerobe 18, 229–234. https://doi.org/10.1016/j.anaerobe.2011.12.006.
Müller, A.L., Kjeldsen, K.U., Rattei, T., Pester, M., Loy, A., 2015. Phylogenetic and environmental diversity of DsrAB-type dissimilatory (bi)sulfite reductases. ISME J. 9, 1152–1165. https://doi.org/10.1038/ismej.2014.208.
Müller, B., Sun, L., Schnürer, A., 2013. First insights into the syntrophic acetate-oxidizing bacteria - a genetic study. Microbiologyopen 2, 35–53. https://doi.org/10.1002/mbo3.50.
Muyzer, G., Stams, A.J.M., 2008. The ecology and biotechnology of sulphate-reducing bacteria. Nat. Rev. Microbiol. 6, 441–454. https://doi.org/10.1038/nrmicro1892.
Ogg, C.D., Patel, B.K.C., 2009. Sporolituus thermophilus gen. nov., sp. nov., a citrate-fermenting thermophilic anaerobic bacterium from geothermal waters of the Great Artesian Basin of Australia. Int. J. Syst. Evol. Microbiol. 59, 2848–2853. https://doi.org/10.1099/ijs.0.010306-0.
Oliveira, J.M.S., Damianovic, M.H.R.Z., Foresti, E., 2022. Two-stage anaerobic digestion system for biotransformation of an azo dye in the presence of sulfate: minimizing competition for reducing equivalents. J. Water Proc. Eng. 47, 102819 https://doi.org/10.1016/j.jwpe.2022.102819.
Oliveira, J.M.S., de Lima e Silva, M.R., Issa, C.G., Corbi, J.J., Damianovic, M.H.R.Z., Foresti, E., 2020. Intermittent aeration strategy for azo dye biodegradation: a suitable alternative to conventional biological treatments? J. Hazard Mater. 385, 9. https://doi.org/10.1016/j.jhazmat.2019.121558.
Özcan, E., Selvi, S.S., Nikerel, E., Teusink, B., Toksoy Öner, E., Çakır, T., 2019. A genome-scale metabolic network of the aroma bacterium Leuconostoc mesenteroides subsp. cremoris. Appl. Microbiol. Biotechnol. 103, 3153–3165. https://doi.org/10.1007/s00253-019-09630-4.
Paliy, O., Shankar, V., 2016. Application of multivariate statistical techniques in microbial ecology. Mol. Ecol. 25, 1032–1057. https://doi.org/10.1111/mec.13536.
Pérez-Díaz, I.M., McFeeters, R.F., 2009. Modification of azo dyes by lactic acid bacteria. J. Appl. Microbiol. 107, 584–589. https://doi.org/10.1111/j.1365-2672.2009.04227.x.
Phugare, S.S., Kalyani, D.C., Surwase, S.N., Jadhav, J.P., 2011. Ecofriendly degradation, decolorization and detoxification of textile effluent by a developed bacterial consortium. Ecotoxicol. Environ. Saf. 74, 1288–1296. https://doi.org/10.1016/j.ecoenv.2011.03.003.
Prato-Garcia, D., Cervantes, F.J., Buitrón, G., 2013. Azo dye decolorization assisted by chemical and biogenic sulfide. J. Hazard Mater. 250–251, 462–468. https://doi.org/10.1016/j.jhazmat.2013.02.025.
Ribeiro, J.C., Mota, V.T., de Oliveira, V.M., Zaiat, M., 2022. Hydrogen and organic acid production from dark fermentation of cheese whey without buffers under mesophilic condition. J. Environ. Manag. 304, 114253 https://doi.org/10.1016/j.jenvman.2021.114253.
Saady, N.M.C., 2013. Homoacetogenesis during hydrogen production by mixed cultures dark fermentation: unresolved challenge. Int. J. Hydrogen Energy 38, 13172–13191. https://doi.org/10.1016/j.ijhydene.2013.07.122.
Santos, A.B., Cervantes, F.J., van Lier, J.B., 2007. Review paper on current technologies for decolourisation of textile wastewaters: perspectives for anaerobic biotechnology. Bioresour. Technol. 98, 2369–2385. https://doi.org/10.1016/j.biortech.2006.11.013.
Saratale, R.G., Gandhi, S.S., Purankar, M.V., Kurade, M.B., Govindwar, S.P., Oh, S.E., Saratale, G.D., 2013. Decolorization and detoxification of sulfonated azo dye C.I. Remazol Red and textile effluent by isolated Lysinibacillus sp. RGS. J. Biosci. Bioeng. 115, 658–667. https://doi.org/10.1016/j.jbiosc.2012.12.009.
Shah, H.N., Gharbia, S.E., 1992. Biochemical and chemical studies on strains designated Prevotella intermedia and proposal of a new pigmented species, Prevotella nigrescens sp. nov. Int. J. Syst. Bacteriol. 42, 542–546. https://doi.org/10.1099/00207713-42-4-542.
Singh, A., Müller, B., Fuxelius, H.H., Schnürer, A., 2019. AcetoBase: a Functional Gene Repository and Database for Formyltetrahydrofolate Synthetase Sequences. Database (Oxford), pp. 1–14. https://doi.org/10.1093/database/baz142, 2019.
Stams, A.J.M., Plugge, C.M., 2009. Electron transfer in syntrophic communities of anaerobic bacteria and archaea. Nat. Rev. Microbiol. 7, 568–577. https://doi.org/10.1038/nrmicro2166.
Stolz, A., 2001. Basic and applied aspects in the microbial degradation of azo dyes. Appl. Microbiol. Biotechnol. 56, 69–80. https://doi.org/10.1007/s002530100686.
Takahashi, N., Yamada, T., 2000. Glucose metabolism by Prevotella intermedia and Prevotella nigrescens. Oral Microbiol. Immunol. 15, 188–195. https://doi.org/10.1034/j.1399-302X.2000.150307.x.
Taylor, K.A.C.C., 1996. A simple colorimetric assay for muramic acid and lactic acid. Appl. Biochem. Biotechnol. Part A Enzyme Eng. Biotechnol. 56, 49–58. https://doi.org/10.1007/BF02787869.
Van Der Zee, F.P., Bisschops, I.A.E., Blanchard, V.G., Bouwman, R.H.M., Lettinga, G., Field, J.A., 2003. The contribution of biotic and abiotic processes during azo dye reduction in anaerobic sludge. Water Res. 37, 3098–3109. https://doi.org/10.1016/S0043-1354(03)00166-0.
Waghmode, T.R., Kurade, M.B., Khandare, R.V., Govindwar, S.P., 2011. A sequential aerobic/microaerophilic decolorization of sulfonated mono azo dye Golden Yellow HER by microbial consortium GG-BL. Int. Biodeterior. Biodegrad. 65, 1024–1034. https://doi.org/10.1016/j.ibiod.2011.08.002.
Waghmode, T.R., Kurade, M.B., Sapkal, R.T., Bhosale, C.H., Jeon, B.H., Govindwar, S.P., 2019. Sequential photocatalysis and biological treatment for the enhanced degradation of the persistent azo dye methyl red. J. Hazard Mater. 115–122. https://doi.org/10.1016/j.jhazmat.2019.03.004.
Wang, J., Yin, Y., 2017. Principle and application of different pretreatment methods for enriching hydrogen-producing bacteria from mixed cultures. Int. J. Hydrogen Energy 42, 4804–4823. https://doi.org/10.1016/j.ijhydene.2017.01.135.
Wang, X., Zhang, Z., Jin, D., Zhou, L., Wu, L., Li, C., Zhao, L., An, W., Chen, Y., 2014. Draft genome sequence of Brachybacterium phenoliresistens strain W13A50, a halotolerant hydrocarbon-degrading bacterium. Genome Announc. 2, 13–14. https://doi.org/10.1128/genomeA.00899-14.
Widdel, F., Pfennig, N., 1982. Studies on dissimilatory sulfate-reducing bacteria that decompose fatty acids II. Incomplete oxidation of propionate by Desulfobulbus propionicus gen. nov., sp. nov. Arch. Microbiol. 131, 360–365. https://doi.org/10.1007/BF00411187.
Wu, J., Eiteman, M.A., Law, S.E., 1998. Evaluation of membrane filtration and ozonation. J. Environ. Eng. 124, 272–277.
Xin, J.Y., Cui, J.R., Niu, J.Z., Hua, S.F., Xia, C.G., Li, S. Ben, Zhu, L.M., 2004. Production of methanol from methane by methanotrophic bacteria. Biocatal. Biotransform. 22, 225–229. https://doi.org/10.1080/10242420412331283305.
You, S.J., Teng, J.Y., 2009. Anaerobic decolorization bacteria for the treatment of azo dye in a sequential anaerobic and aerobic membrane bioreactor. J. Taiwan Inst. Chem. Eng. 40, 500–504. https://doi.org/10.1016/j.jtice.2009.01.007.
Zahran, S.A., Ali-Tammam, M., Ali, A.E., Aziz, R.K., 2021. Compositional variation of the human fecal microbiome in relation to azo-reducing activity: a pilot study. Gut Pathog. 13, 1–12. https://doi.org/10.1186/s13099-021-00454-0.
Zeng, Q., Wang, Y., Zan, F., Khanal, S.K., Hao, T., 2021. Biogenic sulfide for azo dye decolorization from textile dyeing wastewater. Chemosphere 283, 131158. https://doi.org/10.1016/j.chemosphere.2021.131158.
Zimmermann, T., Kulla, H.G., Leisinger, T., 1982. Properties of purified orange I1 azoreductase, the enzyme initiating azo dye degradation by pseudumunas KF46. Eur. J. Biochem. 129, 197–203.